Long-range magnetic couplings between solar flares and coronal mass ejections observed by SDO and STEREO

C. J. Schrijver[1] and A. M. Title[1]

Abstract. The combination of SDO and STEREO observations enable us to view much of the solar surface and atmosphere simultaneously and continuously. These near-global observations often show near-synchronous long-distance interactions between magnetic domains that exhibit flares, eruptions, and frequent minor forms of activity. Here, we analyze a series of flares, filament eruptions, coronal mass ejections, and related events which occurred on 2010/08/01-02. These events extend over a full hemisphere of the Sun, only two-thirds of which is visible from the Earth's perspective. The combination of coronal observations and global field modeling reveals the many connections between these events by magnetic field lines, particularly those at topological divides. We find that all events of substantial coronal activity, including those where flares and eruptions initiate, are connected by a system of separatrices, separators, and quasi-separatrix layers, with little activity within the deep interiors of domains of connectivity. We conclude that for this sequence of events the evolution of field on the hemisphere invisible from Earth's perspective is essential to the evolution, and possibly even to the initiation, of the flares and eruptions over an area that spans at least 180 degrees in longitude. Our findings emphasize that the search for the factors that play a role in the initiation and evolution of eruptive and explosive phenomena, sought after for improved space-weather forecasting, requires knowledge of much, if not all, of the solar surface field.

1. Introduction

The notion of 'sympathetic' events in the solar atmospheric magnetic field goes back at least three quarters of a century [e.g. *Richardson*, 1936, 1951; *Becker*, 1958, and references therein]. The argument whether these were causally linked events rather than chance coincidences has generally revolved around statistical arguments. Even recently, for example, *Moon et al.* [2002] find strong evidence favoring sympathetic flaring (even when no direct evidence exists for interconnecting coronal loops) by analyzing waiting-time distributions between pairs of GOES X-ray flares from different active regions. *Wang et al.* [2001] describe coronal and chromospheric observations of a pair of flares occurring in neighboring active regions in close succession, with evidence of a perturbation associated with the first flare possibly triggering the flare in the adjacent region within an hour of the first event, with a CME-related dimming involving not only the two flaring active regions but also a third located on the opposite side of the equator. *Moon et al.* [2003] pointed out a pair of CMEs from limb active regions in which a CME originating in one active region caused field to be perturbed over another active region, which subsequently produces another CME within 10-20 min. In these and other cases, the hypothetical causal coupling remains rather speculative. Finally, we mention *Wheatland and Craig* [2006] who conclude from their statistical model that 'weak sympathy' is consistent with the observed distributions of flare energy and flare waiting times; in their model, they define 'sympathy' such that "the occurrence of a flare at one magnetic separator increases the probability of flaring at all separators" for some time interval.

The reality of the physical linkages between eruptive and explosive phenomena occurring nearly synchronously in distant regions is important in any study that focuses on the processes involved in catastrophic energy release: is it sufficient to study local properties (from flux emergence to internal field instabilities) or do we also need to study effects from distant fields [as one would in, e.g., the breakout model described by, e.g., *MacNeice et al.*, 2004]. And if the latter, how far do the effects of other active regions reach?

The nature of the physical connection between sympathetic events has been attributed to waves [even applied to sets of stellar flares, e.g. *Mullan*, 1976], direct magnetic connections, or induced currents between neighboring domains of connectivity, preferably running along topological features such as separators, separatrices, and quasi-separatrix layers [*Priest and Titov*, 1996; *Longcope*, 2001; *Démoulin*, 2007; *Masson et al.*, 2009, and references therein]. Here, we study a series of B- and C-class flares, five filament destabilizations or full eruptions, and half a dozen coronal mass ejections occurring on 2010/08/01 by utilizing the remarkable coverage of the solar corona and inner heliosphere enabled by combining observations made by the Solar Dynamics Observatory (SDO) and the two STEREO spacecraft [*Kaiser*, 2005] .

The SDO Atmospheric Imaging Assembly [*Lemen et al.*, 2010] provides a major advance in our ability to observe the solar corona: full-Sun 4096×4096 images with 0.6 arcsec pixels, in temperatures ranging from chromospheric around 10,000 K up to about 10 MK, at a cadence of 12 s, without interruption. This instrument design enables us to trace perturbations over long distances, even if short-lived or occurring at, or changing across, widely different temperatures. At the time of the observations discussed here, the STEREO spacecraft were each approaching quadrature relative to the Sun-Earth line, thus providing perspectives on activity on most of the eastern and western hemispheres as seen from Earth. Moreover, the SDO Helioseismic and Magnetic Imager, combined with a full-sphere flux-transport model and global coronal field modeling reveals the magnetic connections with fair fidelity.

[1]Lockheed Martin Advanced Technology Center, Palo Alto, California, USA.

0148-0227/11/$9.00

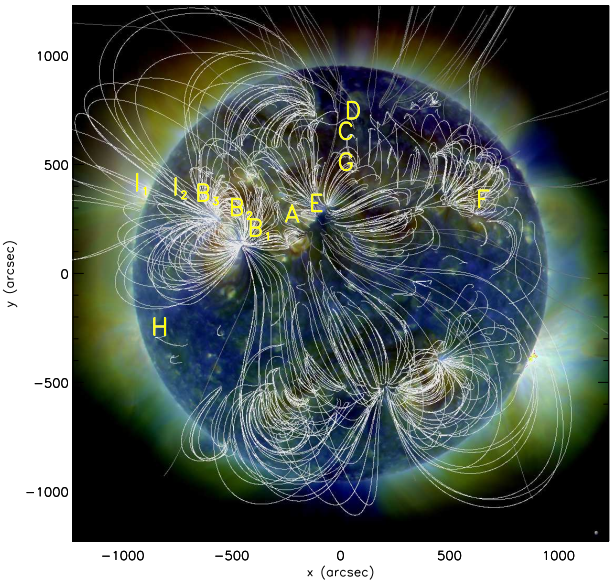

Figure 1. Three-color composite EUV image taken by SDO/AIA at 2010/08/01 06:00 UT. The red, green, and blue components of this image show logarithmically scaled intensities observed in the 211 Å(Fe XIV; ~ 2 MK), 193 Å(Fe XII, ~ 1.5 MK), and 171 Å (Fe IX/X, ~ 1 MK) channels. Select field lines are shown based on a PFSS extrapolation for the full-sphere magnetic field B_1 ($f = 0$; see Sect. 3); white field lines denote closed field, grey field lines are open to the heliosphere beyond the model's source surface. Field-line starting points were selected in proportion to the absolute field strength in the full-sphere map at the resolution of the PFSS model (which includes spherical harmonics up to 192); the same starting positions were used in all images and movies in this study. The Earth is shown to scale in the lower-right corner. Letters denote locations of events discussed in Sect. 2, shown in Figs. 2 and 3, and listed in Table 1.

2. Observations

2.1. Solar Dynamics Observatory

The Solar Dynamic Observatory (SDO) is the first mission to fly in NASA's Living With a Star program. SDO was launched on February 2, 2010, and has been taking observations in science mode since May of that year. The spacecraft is in a Sun-synchronous orbit that allows solar observations continuously except in two relatively short periods each year during which the Earth blocks the view of the Sun during a fraction of the daily orbit. SDO downlinks a continuous data stream of 130 Mbps to a dedicated groundstation in New Mexico. The three instruments provide observations of the solar interior (using helioseismology), surface and its magnetic field (with a visible-light polarimetric imager), and the solar corona out to approximately 1.3 solar radii.

2.1.1. Helioseismic and Magnetic Imager

The line-of-sight (l.o.s.) magnetograms obtained by the Helioseismic and Magnetic Imager [HMI, *Schou et al.*, 2010] on SDO were used in two ways for this study. First, full-disk magnetograms on a cadence of 6 h are assimilated into a model for the full-sphere magnetic field, starting from 2010/07/15 when they began to replace a 14-y series of SOHO/MDI magnetograms in that assimilation code (see Sect. 3 for a description of that code and references).

Second, a series of 2,400 l.o.s. full-disk magnetograms taken at a 45 s cadence was co-aligned with the AIA coronal images (discussed in the next section) for direct comparison over the 30-h interval from 2010/08/01 00:00 UT to 2010/08/02 06:00 UT.

2.1.2. Atmospheric Imaging Assembly

SDO's Atmospheric Imaging Assembly (AIA) carries four (E)UV telescopes. Each of the AIA telescopes supports two separately coated halves of both the primary and secondary mirrors which, in combination with front and back filters and - in one telescope - a mechanical selector, provide access to ten distinct wavelength intervals ranging from a broad-band visible (WL) channel and two UV channels to seven channels in the extreme ultraviolet (EUV).

Around 2010/08/01, the AIA instrument obtained sets of 4096×4096-pixel images (with 0.60 arcsec pixels) in ten wavelength bands at a cadence of 12 s. The UV/WL channel cycled through 1600 Å and 1700 Å images with the broad-band 4500 Å channel taken only once per minute. The seven EUV channels were all on a 12 s cadence: 94 Å Fe XVIII, 133 Å Fe VIII (and, during flaring, Fe XX and XXIII), 171 Å Fe IX/X, 195 Å Fe XII (and, during flaring, Fe XXIV), 211 Å Fe XIV, 304 Å He II, and 335 Å Fe XVI [see *Boerner et al.*, 2010, for the respective thermal response curves]. We selected every 2nd image for each of the 7 EUV channels in the time interval from 2010/08/01 00:00 UT to 2010/08/02 06:00 UT, thus processing a total of 31,500 full-Sun images from the co-aligned set of level 1.5 (i.e., flat-fielded and artifact-corrected) images.

Movies 1a and b (in the on-line material) show the selected time interval in a blend of the 211 Å (red), 193 Å (green), and 171 Å (blue) images, for both the entire northern hemisphere (movie 1a) and for a zoomed-in view at the full AIA pixel resolution for ARs 11092 and 11094 (compare with a selected full-Sun composite shown in Fig. 1, and a full-sphere field map - discussed in Sect. 3 - in Fig. 2 identifying the magnetic active regions on the Sun by their NOAA active region numbers). Movies 2a and b show the same time intervals and fields of view for the chromospheric He II 304 Å channel.

2.2. STEREO

At the time of the events studied here, the two STEREO spacecraft provided near-quadrature observations of the solar corona with the SECCHI EUV and coronagraph imagers [*Howard et al.*, 2008] and of the inner heliosphere with the SECCHI Heliospheric Imagers [*Harrison et al.*, 2005]. On 2010/08/01, STEREO-Behind was trailing the Sun-Earth line (then over Carrington longitude 107.3°) by 70.8° (thus putting it over Carrington longitude 36.5°), and STEREO-Ahead was leading it by 78.9° (over Carrington longitude 186.2°), leaving a wedge of only 30° of the solar surface unobserved.

We used the image sets of both the extreme ultraviolet imagers (EUVI) and of the coronagraphs to assess the timings of events on 2010/08/01 from different perspectives, and to establish whether the erupting filaments were part of coronal mass ejections into the heliosphere and, if so, what the primary direction was for these mass ejections. Moreover, we used a 9-d movie of STEREO-A/B SECCHI/EUVI 171/192/284 Å-channel composites and separately for the 304 Å channel to assess the evolution of the regions behind the solar limbs as viewed by SDO from the Earth perspective.

Movie 3 (in the on-line supporting material) shows the STEREO-A/B (right/left, respectively) EUVI 304 Å images for the 9-d period for all available synchronous image pairs. The contrast in these images is strongly reduced (using a γ value of 0.33) to enhance the quiet-Sun and off-limb features.

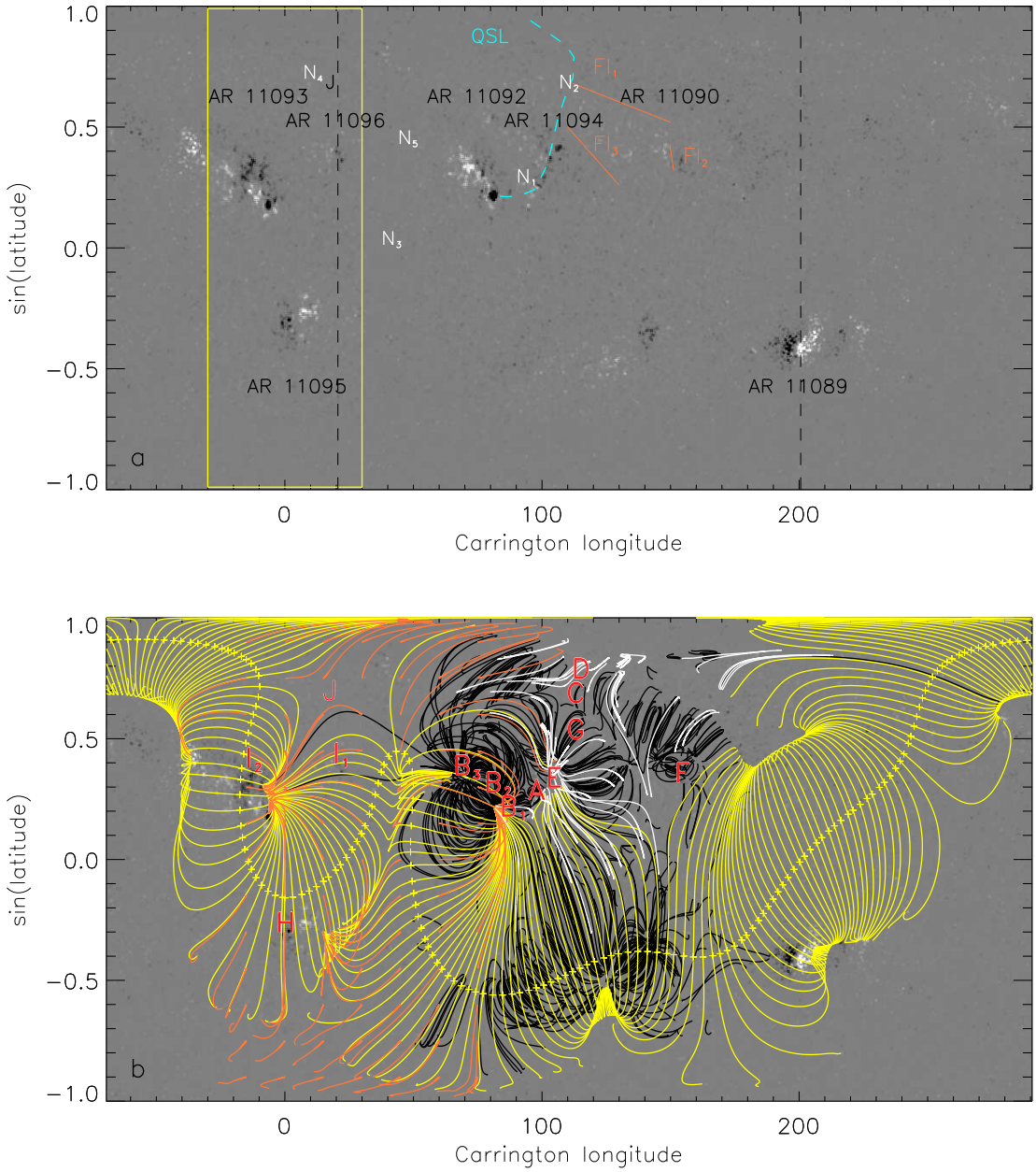

Figure 2. *(a)* Map of the surface magnetic field (for $f = 0.90$, see Sect. 3). The map is centered on the Carrington longitude for 2010/08/01 00:00 UT. The yellow box outlines the area in which the surface field is a weighted average based on past and future observations (see Sect. 3, Eq. 1). Dashed vertical lines show the equatorial longitude of the solar limb. Approximate locations of three erupting filaments are indicated by orange lines. The photospheric track of a primary quasi-separatrix layer is shown by a dashed blue curve. *(b, c, d)* Surface-field maps for $f = 0.60, 0.90, 1.40$, respectively, with projected PFSS model field lines (compare movie 4b). Black field lines show closed field starting from flux concentrations on the front hemisphere as viewed from Earth; white field lines are open to the heliosphere beyond the source surface. Yellow field lines bound the helmet streamer belt, i.e. show the outermost field lines underneath the null line for the radial field at the source surface; the tops of these field lines are marked by yellow pluses. Orange field lines show the connection between the source surface and the photosphere for a grid between Carrington longitudes $-15°$ and $+75°$.

3. Surface and coronal field models

The solar and heliospheric events on 2010/08/01 and 2010/08/02 discussed in the following sections reveal an intricate magnetic connectivity over at least 180° in longitude. In order to demonstrate this, we construct a full-sphere magnetic map and subsequently compute the overlying field under the assumptions made in the potential-field source-surface (PFSS) approximation.

The full-sphere magnetic field is being created by direct insertion of the line-of-sight magnetic field observed within 60° of disk center into an full-sphere field that is evolv-

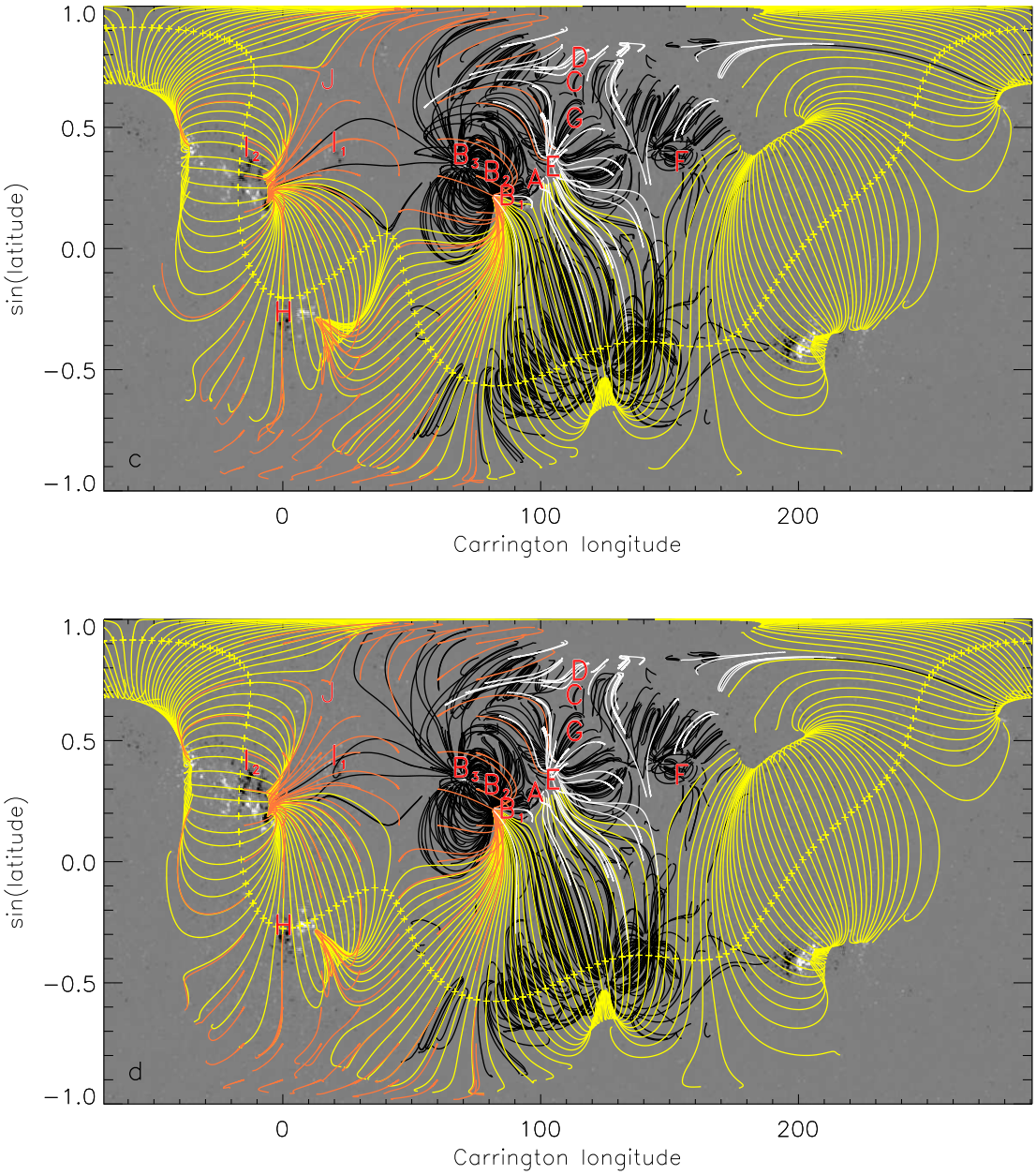

Figure 2. Continued.

ing subject to differential rotation, meridional advection, and random-walk dispersal [*Schrijver and DeRosa*, 2003, http://www.lmsal.com/forecast/]. This model, which has continuously been assimilating SOHO/MDI magnetograms since 1996/07/01 on a 6 h cadence, was switched to assimilation of SDO/HMI line-of-sight field observations starting on 2010/07/15, based on an HMI-to-MDI calibration of $B_{\rm MDI} = 0.18 + 1.322\,B_{\rm HMI}$ (T. Hoeksema and Y. Liu, private communication, with a slightly modified zero-point correction that prevents an apparent monopole from forming in the full-Sun maps; the zero-point offset that we use is consistent with that determined by the HMI team within the uncertainties).

The global coronal field is computed using the SolarSoft PFSS package [described in, e.g., *Schrijver et al.*, 2002], which matches the normal component of the surface magnetic field to a potential field that is forced to become radial at $1.5\,R_\odot$ above the solar surface.

Magnetogram observations taken during the week after 2010/08/01 reveal that new flux had emerged in several locations on the backside hemisphere some time during its two-week period after rotating behind the Sun's western limb. Specifically, new flux emerged into the weakening, pre-existing field configuration to form AR 11093 around Carrington longitude 350°, into a small, unnumbered region around Carrington longitude 20° leading AR 11093 in the northern hemisphere, and to form AR 11095 around Carrington longitude 5° in the southern hemisphere (Fig. 2a). STEREO-Behind SECCHI/EUVI observations show that all three of these bipolar regions already exist by 2010/08/01.

Because we cannot establish the magnetic evolution of these three evolving bipolar regions from available data, we chose to perform the following experiment. We take the full-sphere magnetic field from the assimilation code for

2010/08/01 00:00 UT as one instance of the Sun's global magnetic field, $B_1(\phi, \theta)$. A second instance is computed by taking that field map and replacing the field between Carrington longitudes -30° and 30° (i.e., a 60° strip centered on Carrington longitude 0°) as observed on the front hemisphere on 2010/08/07 00:00 UT to create a second instance of the full-sphere magnetic field, $B_2(\phi, \theta)$.

The field B_1 does not contain information on the newly emerged field behind the eastern limb, while B_2 contains that information after the emerged field has evolved for one week beyond the time interval of interest on 2010/08/01, and we should therefore expect that some of the emerged flux in the bipoles has already cancelled by then during the week of evolution. In order to accommodate for this, we compute a series of magnetic configurations with the PFSS code starting from full-sphere photospheric field configurations given by

$$B_f = (1 - f)B_1 + fB_2 \quad (1)$$

for $f \in [0., 1.5]$ for Carrington longitudes between -30° and 30°, while keeping the surface field outside that longitude interval (shown by the yellow box in Fig. 2a) unchanged. We then compute sets of field lines from fixed starting points on the solar surface, as well as along the cusp of the helmet structure at the foundation of the model's heliospheric current sheet (the null line for the radial field at the source surface), to trace the likely magnetic connections and to assess the large-scale topological structure around 2010/08/01, as discussed in Sect. 5. We take $f = 0.90$ to compute a reference field discussed in Sect. 2. Field-line starting points were selected in proportion to the absolute field strength in the full-sphere map at the resolution of the PFSS model (which includes spherical harmonics up to 192). The same starting positions were used in all images and movies discussed here. Field lines reaching up to the source-surface null line were computed from starting points distributed along the null line and computed from there to the surface by tracing the field in two directions.

4. A time line of events

The surface magnetic field on the hemisphere of the Sun visible from Earth showed little substantial evolution on 2010/08/01. The largest region on the disk, AR 11092, is a region of moderate size, with most of the leading flux concentrated in a large sunspot (near B_1 in Figs. 1 and 2), an extended trailing magnetic plage (B_3) against which a relatively small patch of opposite polarity is located. There is mixed-polarity activity around the leading spot's penumbra, and some flux emergence on the scale of ephemeral regions in multiple places in the immediate vicinity of AR 11092, but there is neither substantial flux emergence nor rapid shearing of the field.

Leading AR 11092 by about 25° is AR 11094, a small, weak, aged region with some mixed polarities. At a comparable latitude further west lie the weak remains of AR 11092. Somewhat above the latitude of these two regions lies an extended quiet-Sun filament, FI_1; its approximate position and the positions of two more filaments, $FI_{2,3}$, are indicated by line segments in the upper-left panel of Fig. 2.

At the eastern limb as seen from Earth lies a small active region, AR 11096, followed by the larger (rejuvenating) AR 11093 some 30° to 50° behind the east limb; AR 11095 lies in the southern hemisphere, some 15° behind the eastern limb. STEREO SECCHI/EUVI observations show that AR 11096 first emerged around 2010/07/28 00 UT, and that the EUV corona over this region brightened markedly over the next day and a half, but with little noticeable growth after about 2010/07/29 12 UT. AR 11093 shows no substantial growth after appearing on the limb as seen from STEREO-B around 2010/07/29, so that we conclude that no significant flux emergence took place in these two regions in the three days leading up to the events on 2010/08/01.

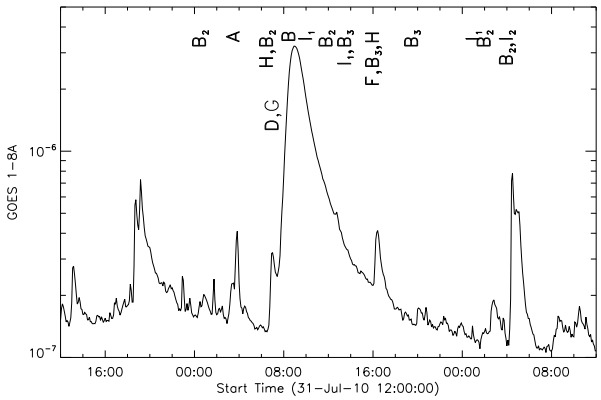

Figure 3. GOES $1 - 8$ Å light curve for a two-day interval centered on 2010/08/01; the plot's vertical scale ranges from the flux levels equivalent to B1 up to C5. Letters denote locations of events discussed in Sect. 2, shown in Figs. 1 and 2, and listed in Table 1.

AR 11095, in contrast, does show increased activity at its north-western edge starting around 2010/07/31 07 UT. The STEREO-B EUVI 304 Å images show frequent flaring and surges throughout the rest of the day, continuing into 2010/08/01.

On the western limb lies AR 11089, which plays no further role in the events on 2010/08/01, being distant and magnetically disconnected from the other active regions mentioned above.

The only other region that appears to have ongoing flux emergence is one on the far side of the Sun, observed at a Carrington longitude of about 275°, just reaching the western limb for STEREO-A at the beginning of 2010/08/01. There is no useful magnetic information on this region until well over a week later (when known as AR 11097), so that we do not include it in the magnetic experiments below.

A time line of events as seen in the SDO/AIA channels (movies 1, 2), the STEREO Ahead/Behind SECCHI/EUVI (movie 3) and HI imagers, and the GOES X-ray monitor is summarized in Table 1 and Fig. 3. Early on 2010/08/01 there is some loop movement (apparent contraction) and minor (low B-class) flaring activity within AR 11092, both in its high loops and SW of the leading spot. More loop contractions over AR 11092 occur around 01 UT. Then, at about 02:17 UT a series of events occurs with the most pronounced brightenings in the southernmost part of AR 11094 near label A in Figs. 1 and 2: the coronal field distorts, there is an apparent eruption associated with some flare ribbons, and a post-eruption arcade forms; these events happen in concert with evolutions near B_3. The eruption from the southern portion of AR 11094 (label A) is associated with a roughly Earth-directed CME that becomes apparent in STEREO-A COR-1 observations around 03 UT.

A few hours later, activity resumes on a larger and more energetic scale. The first signs of this are in the rise of the northernmost extension of filament FI_1 near label C around 05 UT as seen best in STEREO-A SECCHI/EUVI 304 Å images. Around 6:30 UT, this is followed by the activation of a low-lying filament in AR 11092 near $B_{2,3}$. Interestingly, the timing of that activation coincides with a flare-like brightening at the SE limb over AR 11095. Then, towards 07 UT, many things happen side by side: (a) filament FI_1 erupts,

(b) AR 11092 exhibits a C3 flare and coronal reconfiguration, (c) there are faint, transient coronal brightenings near labels D, E, F, and G, and (d) a post-eruption arcade forms over the site of the erupted FI_1.

A few hours later, FI_2 erupts near F, around 15 UT, as transient brightenings occur near A and B_2. In the wake of these events, filament FI_3 erupts in a process lasting from about 19 UT to 21 UT, associated with a composite CME observed by STEREO-A COR-1 that has a component towards the general direction of Earth associated with the eruption of filament FI_3, as well as a component towards the space behind the Sun as viewed from Earth associated with a field eruption northward of ARs 11096 and 11093 (projected as site J when using the observed position over the limb) seen clearly in the over-the-limb coronal deformation in SDO/AIA observations (movie 1a).

5. Discussion

Several of the events of 2010/08/01-02 described above and listed in Table 1 in the solar corona and inner heliosphere show intriguing coincidences in time. Some sets of events occur at widely separated locations on the Sun, as seen clearly in the SDO/AIA movies, and witnessed by the variety of labels (see Figs. 1 and 2b-d) over the GOES light curve shown in Fig. 3.

The coronal magnetic field as computed based on the potential-field source-surface (PFSS) approximation provides unambiguous evidence that these events are, in fact, magnetically related. The PFSS model as shown in Fig. 1 and in panels *b-d* of Fig. 2 reveals a number of the key topological features of the coronal field: arcades over filaments $FI_{1,2}$ (reforming into EUV-bright arcades after the filament eruptions); the magnetic connection of site B_3 to A, I_2, as well as H; and the connection between B_3 and sites of transient brightenings C, D, E, and G.

The topology of the closed field, as outlined by the black lines in Fig. 2 and - in a different projection - by the white lines in Fig. 1 is rather robust to perturbations of the segment of the surface magnetic field which has evolved substantially while on the backside of the Sun, specifically that between Carrington longitudes -30° and $+30^\circ$. As there is no magnetograph access to that side of the Sun before it rotates onto the hemisphere visible from Earth, we investigate the sensitivity to the field in ARs 11093, 11095, and 11096 as described in Sect. 3: we take the field in the above Carrington range and determine the PFSS field for a range of weights f that interpolate between the modeled state based on the on-disk measurements when that region was last on the disk to one week after 2010/08/01. These field configurations are shown in Movies 4a and 4b for $f \in [0\%, 150\%]$, and sampled in Figs. 1 and 2b-d.

Movies 4a,b show, foremost, that the closed field configuration on the front-side of the Sun is relatively insensitive to the field from ARs 11093, 11095, and 11096 behind the western solar limb. This is, of course, not surprising, because those ARs are distant and relatively weak. The movies do readily reveal some topological features, however, by what amounts to a perturbation analysis: note how many of the field lines emanating from the trailing polarity of AR 11092 (near B_3) slide over a quasi-separatrix layer (QSL) that connects sites A, C, D, E, and G; the photospheric footprint of this QSL is marked by the dashed curve in Fig. 2a. Associated with this QSL are two null points (marked $N_{1,2}$), one related to the early eruption near site A, the other over the north-western ends of filaments $FI_{1,3}$ where their eruptions initiate.

Movie 4b, in particular, also clarifies the connection between sites B_2, B_3, and site H of AR 11095: these sites are connected underneath the helmet-streamer structure through a topology related to a null point labeled N_3. The direct linkage of B_1 to H is rather robust, and shows up in Movie 4b for the entire range of f values that we explored. There is an indirect connection of B_3 to H through the null point N_3.

The PFSS models for $f \in [0, 0.78)$ differ fundamentally from those for $f \in [0.78, 1.5]$ for the high coronal field: in the high-f range B_3 is not connected to the null line for the radial field on the source surface (i.e., not connected to the open field into the model's heliosphere), whereas it is in the low-f range. Moreover, in the range of $f \in [0, 0.78)$, the entire domain that incorporates AR 11092 and its connections to the shown QSL westward and to ARs 11093, 11095, and 11096 eastward is enclosed under the helmet-streamer structure that is in part connected to B_3. For $f \in [0.78, 1.5]$, in contrast, the helmet-streamer structure does not appear to close over the extended connectivity domain of AR 11092, or at most involves very little flux, and it is disconnected from B_3. Another change evident in Movie 4b occurs around $f \approx 1.36$ when direct connections between B_3 (AR 11092) and I_1 (AR 11096) show up, although we note that connections probably already exist at lower values of f, but involving so little flux that the relatively few randomly-sampled field lines do not reveal this connection.

These magnetic-field models are consistent with the observed coronal coincidences that link events at $A - I$. The involvement of the eruption over the NE limb around 2010/08/01 21 UT, associated with a CME in the general direction of the backside of the Sun as observed by STEREO-A COR-1 is less clear, but it is interesting that there is a separator set that connects N_1 to N_4 via N_5 so that, even though the eruption of FI_3 occurs outside the domain of connectivity trailing the main QSL shown in Fig. a2, there may be connections related to perturbations of the topology of the field.

6. Conclusions

The potential-field source-surface modeling based on the full-sphere maps of the solar magnetic field for 2010/08/01 reveals the many direct magnetic connections between a series of events that happen at different locations on the Sun. These connections reveal, first, direct linkages between flares or flare-like coronal brightenings in widely separated locations, both between adjacent active regions (such as ARs 11092 and 11094) and between widely separated regions (such as ARs 11092 and 11095, with the latter just beyond the eastern limb). The field model is also highly suggestive of important roles of topological features in the coronal field, such as the null points $N_{1,2}$ (where filament eruptions occur first), and quasi-separatrix layers (such as QSL_1 which contains the nulls $N_{1,2}$ and which also shows coronal brightenings associated with relatively distant flaring including those associated with the C3 flare at B_3). In fact, we conclude that all substantial coronal activity related to the B- and C-class flaring and the field eruptions initiate from a connected network of large-scale separators, separatrices, and quasi-separatrix layers. We interpret this to mean that essentially simultaneous activity or distant events closely spaced in time are effected by either inducing electrical currents along topological divides or by plasma loading of reconnecting field, or both.

The geometry and topology of the closed field for the events analyzed here are relatively insensitive to perturbations in the distant field. This is demonstrated by our experiment in which we vary field behind the eastern solar limb between Carrington longitudes from 90° to 150° east of the central meridian from Earth's perspective. In our experiment, we study a range of field states interpolated from the state it was modeled to be in for 2010/08/01 to the state in which it was observed to be a week (and about 90° of solar

rotation) later on 2010/08/08 (and even somewhat beyond that range) using a relative interpolation factor ranging from 0 to 1.5 (see Eq. 1).

This experiment also readily uncovers the main topological features of the field, for example by showing field lines connecting through null points and sliding along QSLs, as shown in the on-line movies 4a, b. The interpolation experiment for the PFSS field shows that, in contrast to the low-coronal field, the topology of the high-coronal field, in particular that of the helmet-streamer belt and the connectivity of field into the heliosphere, is sensitive to the details of that distant field. For the interpolation factor f in Eq. (1) ranging from 0.69 to 0.77, we see several fundamental changes in the large-scale field (most clearly seen in movie 4b). First, for $f < 0.69$ the domain northward of ARs 11092, 11094, and 11096 lies within the confines of the closed field within the streamer belt, while for higher values of f, the northward excursion of the source-surface null line around Carrington longitude 40° shifts southward, and the helmet structure at these longitudes reaches only up to a latitude of $\sim 17^\circ$ instead of up to $\sim 75^\circ$ at the edge of the north-polar coronal hole. For $f > 0.77$, the source-surface null line migrates so far south that the connection of the trailing polarity of AR 11092 (at label B_3) is disconnected from the streamer belt altogether.

The SDO/AIA observations reveal two classes of connections by the magnetic field that can be differentiated. First, there is the class of transient brightenings (like those at C, D, and F following the C-class flare) which are a consequence of energy or mass being transported along field lines; these events reveal the pathways of the magnetic field, but are not part of the chain of eruptive and explosive phenomena.

Second, there is the class of events where flares and eruptions happen simultaneously or in close succession at magnetically connected sites. We do not have unambiguous evidence that the major changes in the high field revealed by the PFSS-field experiments are related to, and perhaps the cause of, the filament eruptions and coronal mass ejections on 2010/08/01. For one thing, the PFSS model is a good but only approximate description of the evolving global field which should be studied within the MHD approximation. Moreover, as we have no magnetogram measurements of the off-disk regions (ARs 11093, 11095, and 11096) we have no means to feed the required information into a more realistic PFSS model or higher-fidelity MHD model if that were possible at the required resolutions. On the other hand, as we go from $f = 0$ to $f \approx 1$, we view a change in states of the field from one to another which both are likely close to the real coronal state, one before and one after all flux emergence in the three regions on the far side of the Sun: the PFSS model is, after all, highly successful as a field model, even though it should not be expected to describe how and how quickly the field evolves from one state to another.

We can point out that the major topological changes around $f = 0.6 - 0.8$ (i) occur where the largest filament eruptions originate, (ii) take place in a fairly narrow range of f values (particularly for the southward retraction of the helmet streamer seen within a range of values of 0.01 from $f = 0.69$), and (iii) occur around the value of f near the value corresponding to the state suggested by the STEREO SECCHI/EUVI-304 Å observations: the main flux emergence phase in these three off-disk regions is mostly completed, with some residual flux emergence apparently occurring only in AR 11095.

We can interpret the series of eruptions and flares in three different ways. First, it is possible that the events happen independently and that the magnetic field merely acts to transport perturbations over long distances. The synchronicity of the C-class flare at B_3 with the eruption of the large quiet-Sun filament FI_1, and that of the eruption of filament FI_3 and the off-limb coronal perturbation at J appear to argue against that interpretation. Second, it may be that each of these energetic coronal perturbations causes changes in the magnetic field that lead to a destabilization elsewhere, either nearly at the same time or some short time later. Third, it is possible that all of these explosive and eruptive phenomena are the result of destabilizations of local field configurations by an overall change of the large-scale magnetic field; in this interpretation, the events are not a chain in which one induces another, but rather each independently a signature of something larger changing around them.

The latter two interpretations are hard, and perhaps impossible, to clearly differentiate. For both, field changes in one site lead to changes in another. And for both it means that if we wish to understand the destabilization of coronal field configurations, we need to know the field conditions over a large area surrounding any one event: local information will only provide a partial view of what is needed to understand the event. The third interpretation, in which the changing large-scale field destabilizes regional field configurations, is one that is, for example, invoked in the breakout model of filament eruptions and CMEs [e.g. *Gary and Moore*, 2004; *MacNeice et al.*, 2004; *DeVore and Antiochos*, 2008]. Here, an even stronger case is made for the need to know as much of the evolution of the solar surface field as possible.

In summary, we present unambiguous evidence that regions up to 100° away are involved in defining the large-scale coronal field topology for flares and coronal mass ejections. Moreover, we present - as far as we are aware - the first well-documented case that is highly suggestive that the evolution of that distant field, i.e. the flux emergence in one or more of the three active regions behind the eastern limb of the Sun as seen from Earth and SDO, plays an important role in the destabilization of the field involved in a series of CMEs. This work thus stresses the importance of knowing the evolving global solar field as we seek to understand the causes of eruptive and explosive phenomena to improve our ability to forecast space weather.

Acknowledgments. This work was supported by NASA contract NNG04EA00C in support of the SDO Atmospheric Imaging Assembly. We thank the many members of the AIA science, engineering, and data-system teams for their work on designing and operating AIA, and Markus Aschwanden and Jean-Pierre Wuelser for their help with the STEREO observations.

Table 1. *Time line of events, identifying event locations (see labels in Figs. 1 and 2), and the instrument or data set in which the event is best seen (for SDO/AIA, three-channel composite movies were analyzed, such as the 211-193-171 Å set shown in Movies 1a,b).*

Approx. time	Likely location	Notes	Instrument, Channel
2010/08/01:			
00:23UT	B_2	flare-like brightening	AIA094-335-193
01:00UT	south of B_2	some rapid loop motion (contracting?)	AIA211-193-171
01:40UT		start of initial rise into B3 flare	GOES
02:17UT	A	AR 11094 begins to erupt	AIA211-193-171
02:24UT	A	deformation of filament in AR 11094, with some nearby dimmingt	AIA094-335-193
02:40UT	A	filament erupts	AIA304
02:40UT	A	earthward eruption	STEREO-A EUVI195
02:43UT	A	clear signs of ribbons as filament erupts from AR 11094	AIA304
02:51UT	A	clear signs of ribbons as filament in AR 11094erupts	AIA094
02:59UT		start of B2 precursor brightening into short-duration B3 flare.	GOES
03:00UT		first sign of earthward CME	STEREO-A COR1
03:02UT	B_3	activation of N end of active-region filament	AIA211-193-171
03:04UT	A,B_3	rapid eruption from AR 11094 to AR 11092	AIA211-193-171
03:30UT	A	transient dimming south-eastward of AR 11094	AIA30
03:40UT	C	filament FI_1 increases rise speed noticably	AIA211-193-171
05UT	C	large QS filament FI_1 begins rapid rise phase	STEREO-A EUVI195
06:00UT	west of C	apparent acceleration of rise of large northern filament FI_1	AIA304
06:20UT	B_1	initial filament activation	AIA211-193-171
06:30UT	B_1	filament FI_1 activation and apparent rise	AIA304
06:40UT	B_2, H	start of B3 precursor brightening into C3 flare, associated with filament activation in AR 11092 and with a flare in AR 11095	GOES
07:18UT	west of C	apparent ribbons N and S of large rising QS filament FI_1	AIA211-193-171
07:20UT		first signs of off-limb loops opening up	STEREO-A EUVI195
07:21UT		loop opening/deformation (and associated dimming) becomes rapid for SE side of large AR 11092.	AIA211-193-171
07:23UT		minimum brightness between precursor and rise into C3 flare	GOES
07:37UT	A,B	appearance of extended ribbons in large AR 11092, simultaneous with compact ribbon in AR 11094	AIA211-193-171
07:40UT	west of C	post-eruption hot arcade (in 94 Å) begins to form over filament location in large AR 11092	AIA094-335-193
07:48UT	west of C	first hints of post-eruption arcade intensity changes for filament FI_1	AIA211-193-171
07:50UT		first sign of earthward CME	STEREO-A COR1
08:06UT	I	faint changes over NE limb (over AR 11093)	AIA211-193-171
09:00UT		peak brightness for C3 flare.	GOES
09:28UT	B_2	first appearance of bright 'tops' in cooling AR loops	AIA211-193-171
10:32UT	B_3	possible reconnection sequence in southern corona of large AR 11092	AIA211-193-171
12:40UT	B_3	start of ∼B5 brightening on still strong decay flank of C3 flare associated with brightening NE of leading spot]	GOES
13:00UT	B_3	hot 94 Å brightening southward of leading spot with very weak GOES counterpart on flare flank	AIA094-335-193
15:00UT	F	small filament FI_2 rises and erupts	AIA211-193-171
15:13UT	B	hot 94 Å signal in large AR 11092 largely gone	AIA094-335-193
15:16UT	F	post-eruption arcade begins to form at location of erupted FI_2	AIA094-335-193
16:06UT	B_3	hot 94 Å brightening southward of leading spot in large AR 11092	AIA094-335-193
16:08UT	B_3,F,H	start of B4 brightening on late-decay flank of C3 flare [associated with brightening S of leading spot in AR 11092 and/or with offlimb brightening in AR 11095- apparently simultaneously; the decay profile suggests the over-the-limb source as origin. Note: simultaneous brightenings in 94 Å at the leading tail of FI_1 and over FI_2.]	GOES
16:40UT	F	strongest brightening over erupted small filament FI_2	AIA094-335-193
19:30UT	G	southern smaller filament FI_3 appears to rise more rapidly	AIA211-193-171
19:50UT		C3 decay levels out - end of coronal cooling phase?	GOES
19:55UT		slight brightening associated with over-the-limb source AR 11095	GOES
20:05UT		FI_3 begins rapid rise	STEREO-A EUVI195
20:32UT	B_3	possible reconnections and suggestion of southward eruption in large AR 11092 from leading spot	AIA211-193-17
20:36UT	B_3	hot 94 Å brightening southward of leading spot in large AR 11092 (same location as at 16:06UT)	AIA094-335-193
21:00UT	J	first changes in high loops over N-E limb (over AR 11093)	AIA211-193-171
21:10UT		start of CME towards N-W limb, away from Earth.	STEREO-A EUVI195
21:40UT		start of CME towards N-W limb, away from Earth.	STEREO-A COR1
2010/08/02:			
00:49UT	B_3	hot 94 Å brightening westward of leading spot in large AR 11092	AIA094-335-193
04:10UT		start of initial rise into B8 flare	GOES
04:11UT	B_1	hot 94 Å brightening in central region of large AR 11092 (similar to that at 2020/08/01 00:23UT)	AIA094-335-193
04:19UT	H	hot 94 Å brightening in AR 11095	AIA094-335-193
04:20UT	B_2,I_2	start of impulsive rise into B8 flare	GOES

A.M. Title Lockheed Martin Advanced Technology Center, 3251 Hanover Street, Palo Alto CA94304 (title@lmsal.com)

References

Becker, U., Über die Fernauslösung von Eruptionen. Mit 6 Textabbildungen, *Zeitschr. für Astrophysik*, *44*, 243–+, 1958.

Boerner, P., et al., Initial calibration of the atmospheric imaging assembly instrument, *Solar Phys.*, 2010, in press.

Démoulin, P., Where will efficient energy release occur in 3-D magnetic configurations?, *Advances in Space Research*, *39*, 1367–1377, 2007.

DeVore, C. R., and S. K. Antiochos, Homologous Confined Filament Eruptions via Magnetic Breakout, *ApJ*, *680*, 740–756, 2008.

Gary, G. A., and R. L. Moore, Eruption of a Multiple-Turn Helical Magnetic Flux Tube in a Large Flare: Evidence for External and Internal Reconnection That Fits the Breakout Model of Solar Magnetic Eruptions, *ApJ*, *611*, 545–556, 2004.

Harrison, R. A., C. J. Davis, and C. J. Eyles, The STEREO heliospheric imager: how to detect CMEs in the heliosphere, *Advances in Space Research*, *36*, 1512–1523, 2005.

Howard, R. A., et al., Sun Earth Connection Coronal and Heliospheric Investigation (SECCHI), *Space Sci. Rev.*, *136*, 67–115, 2008.

Kaiser, M. L., The STEREO mission: an overview, *Advances in Space Research*, *36*, 1483–1488, 2005.

Lemen, J. R., et al., The atmospheric imaging assembly on the solar dynamics observatory, *Solar Phys.*, 2010, submitted.

Longcope, D. W., Separator current sheets: Generic features in minimum-energy magnetic fields subject to flux constraints, *Physics of Plasmas*, *8*, 5277–5290, 2001.

MacNeice, P., S. K. Antiochos, A. Phillips, D. S. Spicer, C. R. DeVore, and K. Olson, A Numerical Study of the Breakout Model for Coronal Mass Ejection Initiation, *ApJ*, *614*, 1028–1041, 2004.

Masson, S., E. Pariat, G. Aulanier, and C. J. Schrijver, The Nature of Flare Ribbons in Coronal Null-Point Topology, *ApJ*, *700*, 559–578, 2009.

Moon, Y., G. S. Choe, Y. D. Park, H. Wang, P. T. Gallagher, J. Chae, H. S. Yun, and P. R. Goode, Statistical Evidence for Sympathetic Flares, *ApJ*, *574*, 434–439, 2002.

Moon, Y., G. S. Choe, H. Wang, and Y. D. Park, Sympathetic Coronal Mass Ejections, *ApJ*, *588*, 1176–1182, 2003.

Mullan, D. J., Sympathetic stellar flares and electron precipitation as probes of coronal structure in flare stars, *ApJ*, *204*, 530–538, 1976.

Priest, E. R., and V. S. Titov, Magnetic Reconnection at Three-Dimensional Null Points, *Royal Society of London Proceedings Series A*, *354*, 2951–2992, 1996.

Richardson, R. S., *Ann. Rep. Mt. Wison Obs.*, *1935/1936*, 171, 1936.

Richardson, R. S., Characteristics of Solar Flares., *ApJ*, *114*, 356–+, 1951.

Schrijver, C. J., and M. L. DeRosa, Photospheric and heliospheric magnetic fields, *Solar Phys.*, *212*, 165–200, 2003.

Schrijver, C. J., M. L. DeRosa, and A. M. Title, What is missing from our understanding of long-term solar and heliospheric activity?, *ApJ*, *577*, 1006–1012, 2002.

Schou, J. Scherrer, P. H., Bush, R. I., Wachter, R., Couvidat, S., Rabello-Soares, M. C., et al., *Solar Phys.*, submitted, 2010.

Wang, H., J. Chae, V. Yurchyshyn, G. Yang, M. Steinegger, and P. Goode, Inter-Active Region Connection of Sympathetic Flaring on 2000 February 17, *ApJ*, *559*, 1171–1179, 2001.

Wheatland, M. S., and I. J. D. Craig, Including Flare Sympathy in a Model for Solar Flare Statistics, *Solar Phys.*, *238*, 73–86, 2006.

C.J. Schrijver Lockheed Martin Advanced Technology Center, 3251 Hanover Street, Palo Alto CA94304 (schrijver@lmsal.com)

Dynamic content:

Movies 1a, b: [1] SDO/AIA image sequences for 2010/08/01 00:00 UT through 2010/08/02 06:00 UT at 24-s sampling showing blends of the 211 Å (red), 193 Å (green), and 171 Å (blue) exposures. (*a*) shows the northern hemisphere (off-limb signals are enhanced by an exponential filter with a scale height of 75 Mm up to 4 scale heights, leveling off beyond that); (*b*) shows the images zoomed-in at the full AIA pixel resolution for ARs 11092 and 11094 (compare with a selected full-Sun composite shown in Fig. 1, and a full-sphere field map - in Fig. 2a, discussed in Sect. 5 - identifying the magnetic active regions on the Sun by their NOAA active region numbers).

Movies 2a, b: [2] As movies 1a,b, but for the chromospheric He II 304 Å channel.

Movie 3: [3] STEREO-A/B (right/left, respectively) SECCHI/EUVI 304 Å image sequences from approximately 2010/07/25 00 UT through 2010/08/03 00 UT, showing all available synchronous image pairs. The contrast in these images is strongly reduced (using a γ value of 0.33) to enhance the quiet-Sun and off-limb features.

Movies 4a, b: [4] (a) PFSS field lines shown on a 3-channel (211/193/171 Å) composite for 2010/08/01 06 UT. White field lines close back onto the solar surface, while grey field lines connect to the source surface, and are thus open to the model's heliosphere. The movie shows 150 frames for f values (shown in the frames) stepping in increments of 1 % from 0 to 150 (see Sect. 3, and Eq. 1). (b) shows the same model fields (black for closed field lines, white for open field) projected against a synoptic magnetic field. Also shown - in yellow - are field lines that connect the solar surface to the null line for the radial field (the equivalent of the heliospheric current sheet) thus outlining the closed-field streamer belt; yellow plus symbols show the location of the cusp on the source surface. Orange field lines show the connection between the source surface and the photosphere starting from a regularly space grid in both longitude and sin(latitude) between Carrington longitudes $-15°$ and $+75°$.

Notes

1. Also at http://www.lmsal.com/∼schryver/20100801/movie1a.mov, http://www.lmsal.com/∼schryver/20100801/movie1b.mov
2. Also at http://www.lmsal.com/∼schryver/20100801/movie2a.mov, http://www.lmsal.com/∼schryver/20100801/movie2b.mov
3. Also at http://www.lmsal.com/∼schryver/20100801/movie3.mov
4. Also at http://www.lmsal.com/∼schryver/20100801/movie4a.mov, http://www.lmsal.com/∼schryver/20100801/movie4b.mov